Inorg. Chem. **2003**, *42*, 3399–3405

^{31}P Solid State NMR Studies of Metal Selenophosphates Containing $[P_2Se_6]^{4-}$, $[P_4Se_{10}]^{4-}$, $[PSe_4]^{3-}$, $[P_2Se_7]^{4-}$, and $[P_2Se_9]^{4-}$ Ligands

Christian G. Canlas,† Mercouri G. Kanatzidis,† and David P. Weliky*

Department of Chemistry, Michigan State University, East Lansing, Michigan 48824

Received August 10, 2002

^{31}P solid-state nuclear magnetic resonance (NMR) spectra of 12 metal-containing selenophosphates have been examined to distinguish between the $[P_2Se_6]^{4-}$, $[PSe_4]^{3-}$, $[P_4Se_{10}]^{4-}$, $[P_2Se_7]^{4-}$, and $[P_2Se_9]^{4-}$ anions. There is a general correlation between the chemical shifts (CSs) of anions and the presence of a P–P bond. The $[P_2Se_6]^{4-}$ and $[P_4Se_{10}]^{4-}$ anions both contain a P–P bond and resonate between 25 and 95 ppm whereas the $[PSe_4]^{3-}$, $[P_2Se_7]^{4-}$, and $[P_2Se_9]^{4-}$ anions do not contain a P–P bond and resonate between –115 and –30 ppm. The chemical shift anisotropies (CSAs) of compounds containing $[PSe_4]^{3-}$ anions are less than 80 ppm, which is significantly smaller than the CSAs of any of the other anions (range: 135–275 ppm). The smaller CSAs of the $[PSe_4]^{3-}$ anion are likely due to the unique local tetrahedral symmetry of this anion. Spin–lattice relaxation times (T_1) have been determined for the solid compounds and vary between 20 and 3000 s. Unlike the CS, T_1 does not appear to correlate with P–P bonding. ^{31}P NMR is also shown to be a good method for impurity detection and identification in the solid compounds. The results of this study suggest that ^{31}P NMR will be a useful tool for anion identification and quantitation in high-temperature melts.

Introduction

Chalcophosphates are compounds with oxidized phosphorus and at least one P−Q bond, where Q = S or Se. To date, no examples with Q = Te exist in the literature. These compounds exhibit an impressively rich structural diversity because of the large number of stable $[P_yQ_z]^{n-}$ building blocks that can be stabilized and the variety of binding modes in which they can engage.[1] Thio- and selenophosphates are still a relatively small group of compounds compared to the huge class of oxophosphates. The latter are important in the areas of catalysis, ceramics, glasses, and molecular sieves. Many thio- and selenophosphates however also exhibit promising and unique properties such as intercalation chemistry, ion-exchange, and magnetic and optical phenomena.[2]

Among the first chalcophosphate compounds to be studied were the $M_2P_2Q_6$ class (M = divalent metal) which features the ethane-like $[P_2Q_6]^{4-}$ ligand[3] as well as M_3PQ_4[4] and MPQ_4[5] with $[PQ_4]^{3-}$ ligands (M = monovalent or trivalent metal). Various other examples of $[P_yQ_z]^{n-}$-containing materials also exist.[6] Interesting properties and uses exhibited by some $[P_2Q_6]^{4-}$-containing compounds are the following: ferroelectric properties for use in memory devices ($Sn_2P_2S_6$, $CuInP_2S_6$);[7] nonlinear optical properties ($Mn_2P_2S_6$);[2e] photoconductivity ($In_{1.33}P_2Se_6$);[8] cathode material in secondary lithium batteries.[6a,9]

Although many chalcophosphate compounds have been synthesized using the traditional high temperature solid-state

* To whom correspondence should be addressed. E-mail: weliky@cem.msu.edu.

† E-mail: canlas@cem.msu.edu (C.G.C.); kanatzid@cem.msu.edu (M.G.K.).

(1) Kanatzidis, M. G. *Curr. Opin. Solid State Mater. Sci.* **1997**, *2*, 139−149 and references therein.

(2) (a) Clement, R. *J. Chem. Soc., Chem. Commun*. **1980**, 647−648. (b) Michalowicz, A.; Clement, R. *Inorg. Chem*. **1982**, *21*, 3872−3877. (c) Jansen, M.; Henseler, U. *J. Solid State Chem*. **1992**, *99*, 110−119. (d) Bridenbaugh, P. M. *Mater. Res. Bull.* **1973**, *8*, 1055−1060. (e) Lacroix, P. G.; Clement, R.; Nakatani, K.; Zyss, J.; Ledoux, I. *Science* **1994**, *263*, 658−660.

(3) (a) Johnson, J. W. In *Intercalation Chemistry*; Whittingham, M. S., Jacobson, A. J., Eds.; Academic Press Inc: New York, 1982. (b) Ouvrard, G.; Brec, R.; Rouxel, J. *Mater. Res. Bull*. **1985**, *20*, 1181−1189.

(4) Garin, J.; Parthe, E. *Acta Crystallogr*. **1972**, *B28*, 3672−3674.

(5) Le Rolland, B.; McMillan, P.; Molinie, P.; Colombet, P. *Eur. J. Solid State Inorg. Chem.* **1990**, *27*, 715−724.

(6) (a) Evain, M.; Brec, R.; Whangbo, M.-H. *J. Solid State Chem*. **1987**, *71*, 244−262. (b) Evain, M.; Lee, S.; Queignec, M.; Brec, R. *J. Solid State Chem.* **1987**, *71*, 139−153. (c) Evain, M.; Queignec, M.; Brec, R.; Rouxel, J. *J. Solid State Chem.* **1985**, *56*, 148−157.

(7) (a) Carpentier, C. D.; Nitsche, R. *Mater. Res. Bull*. **1974**, *9*, 1097−1100. (b) Rogach, E. D.; Arnautova, E. A.; Savchenko, E. A.; Korchagina, N. A.; Barinov, L. P. *Zh. Tek. Fiz.* **1991**, *61*, 164−167. (c) Bourdon, X.; Grimmer, A.-R.; Cajipe, V. B. *Chem. Mater*. **1999**, *11*, 2680−2686.

10.1021/ic025946j CCC: $25.00
Published on Web 04/12/2003

method in which the corresponding metals and chalcophosphates are combined stoichiometrically at high temperature, there was also a crucial role for poly(chalcophosphate) fluxes.[1] In flux methodology, molten salts generate low-melting $[P_yQ_z]^{n-}$ ligands which then react with metal ions. Because of the low temperature, thermodynamically stable phases can be avoided and metastable or kinetically stable phases can be made.

There has been one NMR study of flux composition by Eckert et al. In a Li−P−Se melt at $T > 370$ °C, the high-temperature ^{31}P NMR spectrum provided evidence for the existence of the stable phases $Li_4P_2Se_6$ and Li_7PSe_6. NMR spectra of the solid products showed that $Li_4P_2Se_6$ contains the $[P_2Se_6]^{4-}$ unit, while Li_7PSe_6 contains $[PSe_4]^{3-}$ and Se^{2-} units.[10] There have been additional ^{31}P NMR studies of ternary phases of crystalline solid products formed from direct combination of M + P + Se (M = Cu, Ag, Cd, Hg, Pb, Sn, Ca, and In), and it was reported that the M−P−Se system has much less structural anion variety compared to the ternary sulfide systems.[11] In these direct combination melts, high-temperature NMR data were consistent with the presence of only two anions, $[P_2Se_6]^{4-}$ and $[PSe_4]^{3-}$. Eckert et al. have also studied pure P−S and P−Se glasses with high-temperature ^{31}P and ^{77}Se NMR.[12]

Given the plethora of new chalcophosphate phases discovered in the past decade, and the variety of novel structural types, bonding modes, and chalcophosphate anions, it would be particularly desirable to study the NMR properties of these phases. Given that studies of this type are scarce, a wide compilation of NMR data on $[P_xQ_y]^{n-}$ anions and appropriate correlations with structure and bonding should yield considerable new insights in understanding and characterizing chalcophosphate compounds. Here we present the first solid state ^{31}P NMR investigations of several recently discovered phases containing known anions such as $[P_2Se_6]^{4-}$ ($K_2CdP_2Se_6$, and $Rb_2CdP_2Se_6$) and $[PSe_4]^{3-}$ ($KPbPSe_4$, $RbPbPSe_4$, and $K_4Pb(PSe_4)_2$) in bonding modes and arrangements different from those studied in the past, as well as new anions such as $[P_4Se_{10}]^{4-}$ ($K_2Cu_2P_4Se_{10}$), $[P_2Se_7]^{4-}$ ($Rb_4Ti_2P_6Se_{25}$), and $[P_2Se_9]^{4-}$ ($Cs_4P_2Se_9$, and $Rb_4Ti_2P_6Se_{25}$).[13]

Experimental Section

Synthesis. P_2Se_5 was prepared by reacting stoichiometric amounts of the elements in an evacuated Pyrex tube at 300 °C for 1 day, followed by a cool-down to 50 °C over 2 h. Purity was assessed by X-ray powder diffraction analysis.

$Ag_4P_2Se_6$,[14] $Pb_2P_2Se_6$,[15] and Cu_3PSe_4[16] were prepared by reacting stoichiometric amounts of the metal (Ag, Pb, Cu) with P_2Se_5 and elemental Se. The reaction took place in an evacuated quartz tube at 600 °C for 1 day followed by a cool-down to 50 °C over 12 h.

$KPbPSe_4$ and $RbPbPSe_4$[17] were prepared from stoichiometric amounts of the alkali selenide (K_2Se or Rb_2Se), Pb metal, P_2Se_5, and elemental Se. The reactants were heated in an evacuted quartz tube at 600 °C for 1 day and cooled to 50 °C over 12 h.

$K_2Cu_2P_4Se_{10}$[18] was prepared from 0.3 mmol of Cu, 0.9 mmol of P, 0.3 mmol of K_2Se, and 2.4 mmol of Se. The reactants were heated at 570 °C for 2 days followed by cooling at 21 °C/h. The residual flux was removed with *N*,*N*-dimethylformamide. After the remaining solid was washed with diethyl ether, red irregularly shaped crystals were obtained which were stable in air and water.

$K_4Pb(PSe_4)_2$[17] was prepared as orange crystals from 0.15 mmol of Pb, 0.225 mmol of P_2Se_5, 0.6 mmol of K_2Se, and 1.5 mmol of Se. The reactants were heated at 500 °C for 3 days followed by cooling at 10 °C/h.

$Rb_2CdP_2Se_6$ and $K_2CdP_2Se_6$[19] were prepared from 0.25 mmol of Cd, 0.75 mmol of P_2Se_5, 1.0 mmol of Rb_2Se or K_2Se, and 2.5 mmol of Se with the same heating profile as was used for $K_4Pb(PSe_4)_2$. The residual flux was removed with *N*,*N*-dimethylformamide. After the remaining solid was washed with diethyl ether, dark yellow rodlike crystals were obtained, which were stable in air and water.

$Cs_4P_2Se_9$[20] was synthesized from a mixture of 0.45 mmol of P_2Se_5, 1.20 mmol of Cs_2Se, and 3.0 mmol of Se. The reactants were sealed under vacuum in a Pyrex tube and heated to 490 °C for 4 days followed by cooling to 150 °C at 10 °C/h. The product crystals were red and were sensitive to air and water.

$Rb_4Ti_2P_6Se_{25}$[20] was synthesized from a mixture of 0.2 mmol of Ti, 0.4 mmol of P_2Se_5, 0.4 mmol of Rb_2Se, and 2 mmol of Se. The reactants were sealed under vacuum in a Pyrex tube and heated according to the same heating profile as $Cs_4P_2Se_9$. The residual flux was removed with *N*,*N*-dimethylformamide. After the remaining solid was washed with ether, black crystals were formed, which were stable in air and water. The original goal of this synthesis was to make $RbTiPSe_5$, but powder X-ray diffraction on the whole sample and elemental analysis on selected crystals showed that $Rb_4Ti_2P_6Se_{25}$ was the only crystalline product.

Physical Measurements. (a) Elemental Analysis. The elemental compositions of selected crystals of $Rb_4Ti_2P_6Se_{25}$ and $K_2Cu_2P_4Se_{10}$ were confirmed by semiquantitative elemental analysis using energy dispersive spectroscopy (EDS) on a JEOL 6400 scanning electron microscope equipped with a Tracor Noran detector.

(b) Powder X-ray Diffraction. Powder X-ray diffraction (PXRD) analyses were performed using an INEL CPS 120 powder diffractometer with graphite-monochromatized Cu Kα radiation. To assess sample purity, we visually compared the experimental powder diffraction pattern to a pattern calculated from a single-

(8) (a) Katty, A.; Soled, S.; Wold, A. *Mater. Res. Bull.* **1977**, *12*, 663−666. (b) Etman, M.; Katty, A.; Levy-Clement, C.; Lemasson, P. *Mater. Res. Bull.* **1982**, *17*, 579−584.

(9) (a) Thompson, A. H.; Whittingham, M. S. U.S. Patent 4,049,879, 1997. (b) Brec, R.; Le Mehaute, A. Fr. Patent 7,704,519, 1997. (c) Thompson, A. H.; Whittingham, M. S. *Mater. Res. Bull.* **1977**, *12*, 741.

(10) Francisco, R. H. P.; Tepe, T.; Eckert, H. *J. Solid State Chem.* **1993**, *107*, 452−459.

(11) Francisco, R. H. P.; Eckert, H. *J. Solid State Chem.* **1994**, *112*, 270−276.

(12) (a) Mutolo, P. F.; Witschas, M.; Regelsky, G.; Schmedt auf der Guenne, J.; Eckert,H. *J. Non-Cryst. Solids* **1999**, *256*, *257*, 63−72. (b) Maxwell, R.; Eckert, H. *J. Phys. Chem.* **1995**, *99*, 4768−4778. (c) Maxwell, R.; Eckert, H. *J. Am. Chem. Soc.* **1994**, *116*, 682−689. (d) Maxwell, R.; Eckert, H. *J. Am. Chem. Soc.* **1993**, *115*, 4747−4753.

(13) $Rb_4Ti_2P_6Se_{25}$ has also been examined by H. Eckert and G. Regelsky (private communication).

(14) Chondroudis, K.; McCarthy, T.; Kanatzidis, M. G. *Inorg. Chem.* **1996**, *35*, 840−844.

(15) Toffoli, P. P.; Khodadad, P.; Rodier, N. *Acta Crystallogr.* **1978**, *B34*, 1779−1781.

(16) Yun, H.; Ibers, J. A. *Acta Crystallogr.* **1987**, *C43*, 2002−2004.

(17) Garin, J.; Parthe, E. *Acta Crystallogr.* **1972**, *B28*, 3672.

(18) Chondroudis, K.; Kanatzidis, M. G. *Inorg. Chem.* **1998**, *37*, 2098−2099.

(19) Chondroudis, K.; Kanatzidis, M. G. *J. Solid State Chem.* **1998**, *138*, 321−328.

(20) Chondroudis, K.; Kanatzidis, M. G. *Inorg. Chem.* **1995**, *34*, 5401−5402.

crystal structure. Visual inspection using a light microscope was also performed to assess the crystallinity of the sample.

(c) NMR. The room-temperature solid-state NMR measurements of these compounds were taken on a 9.4 T NMR spectrometer (Varian Infinity Plus) using a double resonance magic angle spinning (MAS) probe. Samples were spun at frequencies between 7 and 15 kHz using zirconia rotors of 4 mm outer diameter and 50 μL sample volume. Bloch decay spectra were taken with the excitation/detection channel tuned to ^{31}P at 161.39 MHz, a 4.5 μs 90° pulse (calibrated to $\pm$0.1 μs with 85% H_3PO_4), and a relaxation delay between 5 and 15000 s. Each spectrum was processed with $\leq$100 Hz line broadening and up to a 10th order polynomial baseline correction. The spectra were referenced using 85% H_3PO_4 at 0 ppm. If the relaxation delay prior to pulsing is comparable to or longer than ^{31}P longitudinal relaxation time, a high signal-to-noise spectrum can be obtained with one scan on $\sim$100 mg of material.

Best-fit chemical shift anisotropy (CSA) principal values were calculated with a Herzfeld−Berger computer program whose inputs were the ^{31}P NMR and spinning frequencies and the experimental peak intensities of the isotropic resonance and the spinning sidebands.[21] For compounds containing the $[P_2Se_6]^{4-}$, $[P_4Se_{10}]^{4-}$, or $[P_2Se_9]^{4-}$ anion, there were typically four spinning sidebands in a spectrum, and for compounds containing the $[P_2Se_7]^{4-}$ or $[PSe_4]^{3-}$ anion, there were typically two spinning sidebands in a spectrum. To quantitatively evaluate uncertainties in CSA principal values, spectra for each compound were typically taken at two or more spinning frequencies and the CSA principal value analysis was done at each frequency. Uncertainty was also evaluated by doing analyses with spectral intensities changed by amounts comparable to the spectral noise. Comparison of the principal values derived from the different analyses showed that the greatest variation of a best-fit principal value was $\sim$20 ppm.

We also calculated an overall CSA value by taking the difference between the two extreme CSA principal values. This overall CSA gives the approximate range of ^{31}P CSs which would be observed in the static powder pattern, i.e., for consideration of all possible orientations of the selenophosphate unit cell relative to the magnetic field direction. The CSA is also a measure of the shielding field range for the ^{31}P. When analyses were compared between spectra taken at different spinning frequencies or between spectra whose peak intensities were changed by amounts comparable to the spectral noise, the greatest variation of CSA was $\sim$20 ppm.

Each compound ^{31}P longitudinal relaxation time (T_1) was determined by fitting the following equation:

$$S(\tau) = S_0(1 - e^{-\tau/T_1}) \quad (1)$$

Here τ is the relaxation delay time before pulsing, $S(\tau)$ is the integrated signal intensity (sum of isotropic peak and spinning sidebands), and S_0 is a fitting parameter representing the signal intensity at infinite τ. Before each τ, the magnetization was nulled with a 90° pulse and subsequent rapid transverse dephasing. For each compound, there were typically at least two data sets and the experimental T_1 uncertainty was calculated from the variation in best-fit T_1 values among the different data sets. This variation was generally larger than the fitting uncertainty in the T_1 value of a single data set.

Results and Discussion

Figure 1 summarizes the structural schemes for the different selenophosphate anions examined in this paper. ^{31}P

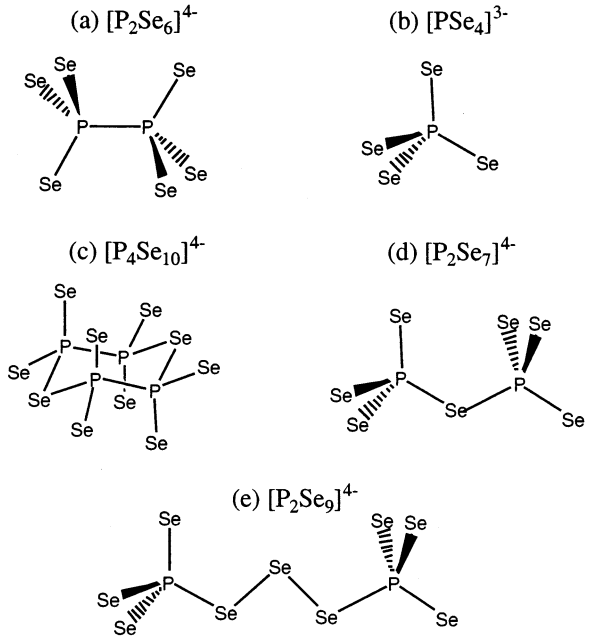

Figure 1. Schematic structures for the various $[P_xSe_y]^{n-}$ anions examined in this work.

solid-state NMR spectra are presented in Figure 2, and the measured chemical shifts (CSs), CSA principal values, CSAs, and T_1 values are presented in Table 1. Figure 3 displays an experimental $Rb_2CdP_2Se_6$ spectrum as well as a simulated stick spectrum calculated from its best-fit CSA principal values. The agreement between intensities in the experimental and simulated spectra is a qualitative illustration of the accuracy of the principal value analysis. Figure 4 displays examples of experimental and best-fit buildup curves which were used to derive T_1 values. In general, there was good agreement between the experimental and fitted curves. Finally, it is noted that, in some spectra, there were resolved spectral splittings due to scalar (spin−spin) couplings which are isotropic and are not averaged by MAS. For $K_2Cu_2P_4Se_{10}$, Ag_7PSe_6, $KPbPSe_4$, $RbPbPSe_4$, $K_4Pb(PSe_4)_2$, and $Cs_4P_2Se_9$, the splittings were due to ^{31}P−^{77}Se scalar couplings while, for $Ag_4P_2Se_6$, the splittings were due to ^{31}P−^{31}P scalar couplings.

$[P_2Se_6]^{4-}$. The ^{31}P CSs of selenophosphates containing $[P_2Se_6]^{4-}$ anions occur downfield in the 25−95 ppm range. Their CSAs range from 145 to 230 ppm. One of the compounds, $Pb_2P_2Se_6$, has monoclinic symmetry so that the two P atoms are crystallographically and magnetically equivalent and have the same CS.[11] Two of the compounds, $Rb_2CdP_2Se_6$ and $K_2CdP_2Se_6$, are isostructural, and this is reflected in CSs and CSAs which are within 1.3 and 9 ppm of one another, respectively. These two compounds also have the shortest T_1 values of any of the selenophosphate compounds in this study. For $Ag_4P_2Se_6$, the two P atoms in the $[P_2Se_6]^{4-}$ anion are crystallographically and magnetically inequivalent and this is reflected in distinct CSs at 77.6 and 91.8 ppm.[11] In addition, the P atoms experience a P−P scalar coupling of 426 Hz. These CS and scalar coupling assignments were confirmed by measurements on a 7 T NMR. There is an additional peak in the spectrum at −51.9 ppm

(21) Herzfeld, J.; Berger, A. E. *J. Chem. Phys.* **1980**, *73*, 6021−6030.

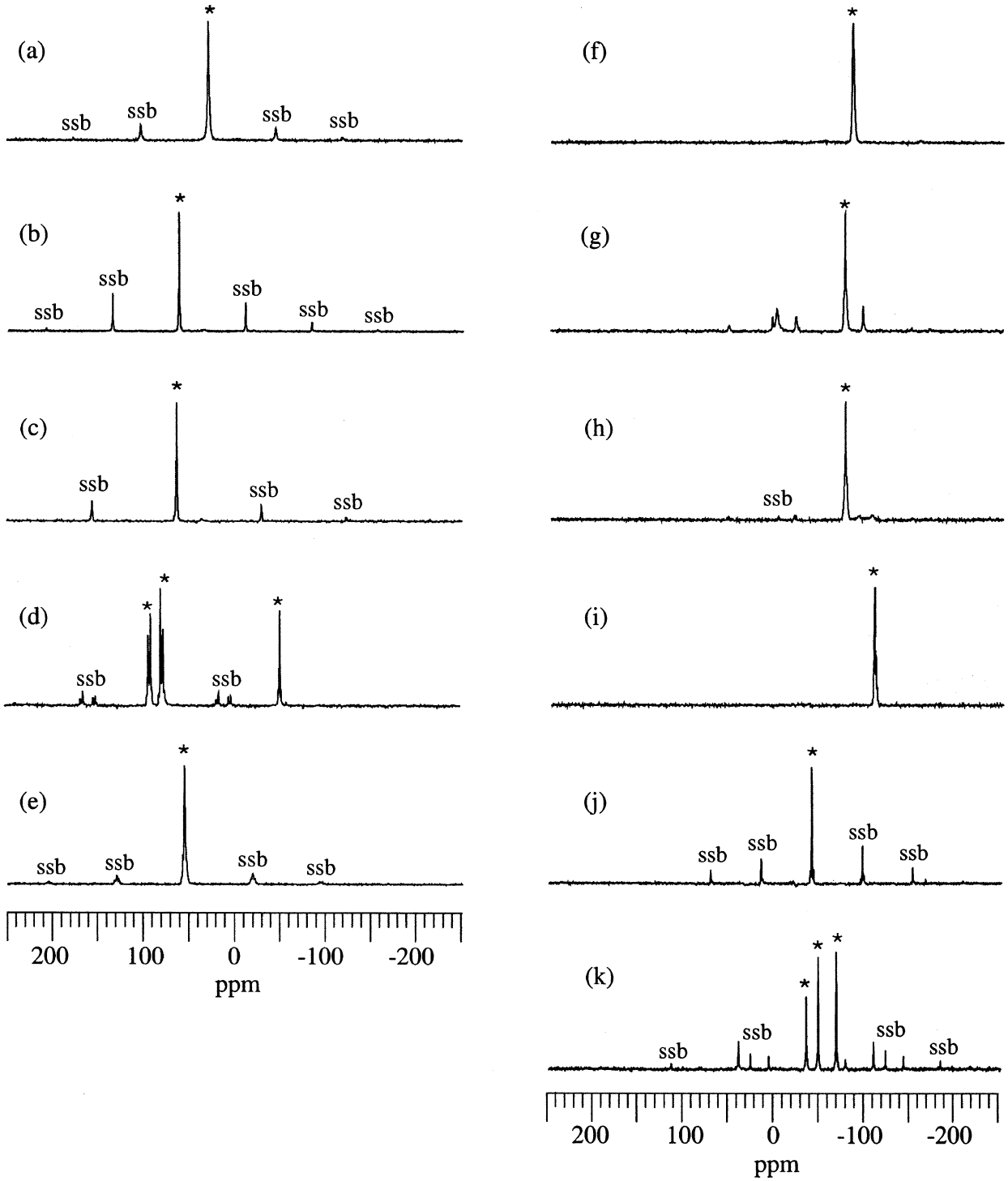

Figure 2. ^{31}P solid-state MAS NMR spectra of selenophosphate compounds. Each spectrum represents a single Bloch decay acquired after a delay time much longer than the ^{31}P T_1 of the compound. Each spectrum was processed with ≤100 Hz line broadening and up to a 10th order polynomial baseline correction. Chemical shift referencing was done using 85% H_3PO_4 at 0 ppm. The isotropic peaks are indicated by asterisks (*), and spinning sidebands are marked as "ssb". (a) $Pb_2P_2Se_6$. The isotropic peak is at 29.1 ppm, the spinning frequency is 12 kHz, and the delay time is 10000 s. (b) $Rb_2CdP_2Se_6$. The isotropic peak is at 62.0 ppm, the spinning frequency is 12 kHz, and the delay time is 300 s. (c) $K_2CdP_2Se_6$. The isotropic peak is at 63.3 ppm, the spinning frequency is 15 kHz, and the delay time is 300 s. (d) $Ag_4P_2Se_6$. The spinning frequency is 12 kHz, and the delay time is 15000 s. There are isotropic peaks at 77.6 and 91.8 ppm which represent the averages of doublets whose splitting is due to P−P *J*-coupling. For $Ag_4P_2Se_6$, the two P atoms in the $[P_2Se_6]^{4-}$ anion are crystallographically and magnetically inequivalent and this is reflected in the observation of two CSs.[11] The peak at −51.9 ppm corresponds to Ag_7PSe_6, which cocrystallized as an impurity with $Ag_4P_2Se_6$. (e) $K_2Cu_2P_4Se_{10}$. The isotropic peak is at 55.7 ppm, the spinning frequency is 12 kHz, and the delay time is 15000 s. (f) Cu_3PSe_4. The isotropic peak is at −83.3 ppm, the spinning frequency is 12 kHz, and the delay time is 10000 s. (g) $RbPbPSe_4$. The isotropic peak is at −74.9 ppm, the spinning frequency is 12 kHz, and the delay time is 15000 s. Some impurity phases can also be seen in the NMR spectrum. (h) $KPbPSe_4$. The isotropic peak is at −74.3 ppm, the spinning frequency is 12 kHz, and the delay time is 5500 s. Some impurity phases can also be seen in the NMR spectrum. (i) $K_4Pb(PSe_4)_2$. The isotropic peak is at −113.2 ppm, the spinning frequency is 12 kHz, and the pulse delay is 6000 s. (j) $Cs_4P_2Se_9$. The isotropic peak is at −39.9 ppm, the spinning frequency is 9 kHz, and the pulse delay is 4200 s. (k) $Rb_4Ti_2P_6Se_{25}$. The isotropic peaks are at −34.6, −47.6, and −67.7 ppm, the spinning frequency is 12 kHz, and the delay time is 6000 s. The first two peaks correspond to the two $[P_2Se_9]^{4-}$ units, and the last peak corresponds to the $[P_2Se_7]^{4-}$ unit.

Table 1. ^{31}P Chemical Shift (CS), Chemical Shift Anisotropy (CSA), and T_1 Measurements for Metal Selenophosphates

			CSA principal values (ppm)[b]				
selenophosphate	anion type	CS (ppm)[a]	δ_{11}	δ_{22}	δ_{33}	CSA (ppm)[c]	T_1 (s)[d]
$Pb_2P_2Se_6$	$P_2Se_6^{4-}$	29.1	97	49	−59	156	1700 (100)
$Rb_2CdP_2Se_6$	$P_2Se_6^{4-}$	62.0	161	93	−69	230	80 (5)
$K_2CdP_2Se_6$	$P_2Se_6^{4-}$	63.3	155	101	−66	221	23 (2)
$Ag_4P_2Se_6$	$P_2Se_6^{4-}$	77.6	152	73	7	145	3000 (200)
		91.8	166	106	3	164	
$K_2Cu_2P_4Se_{10}$	$P_4Se_{10}^{4-}$	55.7	126	53	−12	138	1050 (100)
Ag_7PSe_6	PSe_4^{3-}, Se^{2-}	−51.9	nd[f]	nd	nd	nd	1500 (50)
Cu_3PSe_4	PSe_4^{3-}	−83.3	nd	nd	nd	nd	300 (10)
$RbPbPSe_4$	PSe_4^{3-}	−74.9	−50	−61	−114	64	970 (75)
$KPbPSe_4$	PSe_4^{3-}	−74.3	−53	−54	−118	65	1080 (100)
$K_4Pb(PSe_4)_2$	PSe_4^{3-}	−113.2	−80	−113	−147	67	1250 (100)
$Cs_4P_2Se_9$	$P_2Se_9^{4-}$	−39.9	60	−59	−121	181	800 (200)
$Rb_4Ti_2P_6Se_{25}$[e]	$P_2Se_9^{4-}$	−34.6	100	−30	−174	274	540 (50)
	$P_2Se_9^{4-}$	−47.6	52	−66	−129	181	630 (40)
	$P_2Se_7^{4-}$	−67.7	11	−65	−149	160	690 (50)

[a] Uncertainties are ∼±0.5 ppm. [b] Maximum uncertainties are ∼±20 ppm. [c] CSA = $\delta_{11} - \delta_{33}$, i.e., the approximate overall width of the static CS powder pattern. Maximum CSA uncertainties are ∼±20 ppm. [d] Uncertainties are given in parentheses. [e] CS assignments were based on ref 23b. [f] nd = not determined because of negligible spinning sideband intensity.

which is assigned to a 20% Ag_7PSe_6 impurity.[22] Ag_7PSe_6 has the form $Ag_7(PSe_4^{3-})(Se^{2-})_2$, and its CS is distinct from those found for compounds containing $[P_2Se_6]^{4-}$ units.

$[P_4Se_{10}]^{4-}$. The unique $[P_4Se_{10}]^{4-}$ anion was discovered in $K_2Cu_2P_4Se_{10}$,[18] and it essentially derives from the fusion of two $[P_2Se_6]^{4-}$ units followed by the elimination of two Se^{2-} anions. As a ligand, it possesses eight terminal Se sites available for coordination (cf. Figure 1e). $K_2Cu_2P_4Se_{10}$ has two crystallographically inequivalent P atoms in its crystal structure, but the ^{31}P NMR spectrum has only a single isotropic peak at 55.7 ppm. To understand this apparent discrepancy, the environments around the two P atoms were visually examined in the crystal structure. It was observed that the local interatomic bond distances and angles were substantially the same for the two atoms, which results in chemically and magnetically equivalent P atoms. The $[P_4Se_{10}]^{4-}$ anion is similar to the $[P_2Se_6]^{4-}$ anion in that it contains P−P bonds and tetravalent P. These structural similarities help to explain the observation that the CS of $K_2Cu_2P_4Se_{10}$ (55.7 ppm) is within the CS range of $[P_2Se_6]^{4-}$ anions. The CSA of $K_2Cu_2P_4Se_{10}$ (138 ppm) is also close to the CSAs found for compounds with $[P_2Se_6]^{4-}$ anions. In $K_2Cu_2P_4Se_{10}$, the resolved P−Se scalar coupling is 694 Hz.

$[PSe_4]^{3-}$. The ^{31}P CSs of selenophosphates containing $[PSe_4]^{3-}$ units occur upfield in the −115 to −50 ppm range. Their CSAs are <80 ppm, which is significantly smaller than those observed for $[P_2Se_6]^{4-}$ anions, and likely reflects the high tetrahedral symmetry of $[PSe_4]^{3-}$ units. One of the compounds, Cu_3PSe_4, has a wurtzite-related normal tetrahedral structure with crystallographically equivalent P atoms in its unit cell and a single CS.[11] Two of the compounds, $KPbPSe_4$ and $RbPbPSe_4$, have the same orthorhombic crystal structure with crystallographically equivalent P atoms in their unit cells. This leads to a single CS for each compound which differ by only 0.6 ppm. Both $KPbPSe_4$ and $RbPbPSe_4$ exhibit a resolved P−Se scalar coupling of 435 Hz. $K_4Pb(PSe_4)_2$ has a structure consisting of two $[PSe_4]^{3-}$ ligands which bridge adjacent Pb atoms. All P atoms are crystallographically equivalent, leading to a single CS and a resolved P−Se scalar coupling of 432 Hz. The P−Se scalar coupling of Ag_7PSe_6 is 490 Hz.

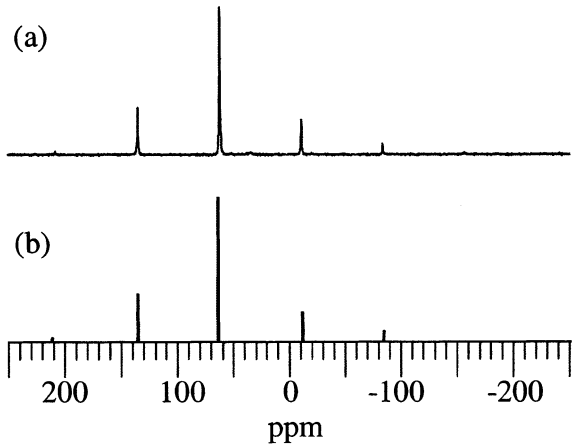

Figure 3. (a) Experimental $Rb_2CdP_2Se_6$ spectrum at 11.76 kHz MAS frequency and (b) simulated stick spectrum calculated from the best-fit CSA principal values. The spectra were scaled so that their isotropic peak intensities were equal. The principal values were derived from Herzfeld−Berger fitting of the experimental isotropic and spinning sideband peak intensities.

$[P_2Se_9]^{4-}$. Two compounds, $Cs_4P_2Se_9$ and $Rb_4Ti_2P_6Se_{25}$, contain the $[P_2Se_9]^{4-}$ anion. This ligand is structurally composed of two Se-sharing $[PSe_4]^{3-}$ subunits. Thus, it is reasonable that the CSs observed for this ligand (−50 to −35 ppm) are close to the CS range observed for compounds containing single $[PSe_4]^{3-}$ anions. The CSAs of $[P_2Se_9]^{4-}$ anions are comparable to those observed for $[P_2Se_6]^{4-}$ anions and are significantly larger than those observed for $[PSe_4]^{3-}$ anions. The latter finding likely reflects the lower symmetry of $[P_2Se_9]^{4-}$ units relative to tetrahedral $[PSe_4]^{3-}$ units. In $Cs_4P_2Se_9$, the resolved P−Se scalar coupling is 530 Hz.

$[P_2Se_7]^{4-}$. $Rb_4Ti_2P_6Se_{25}$ also contains the $[P_2Se_7]^{4-}$ ligand, which is structurally composed of two $[PSe_4]^{3-}$ sharing a common Se. The CS of the $[P_2Se_7]^{4-}$ anion is −67.7 ppm and is within the CS range of $[PSe_4]^{3-}$ anions. The CSA of the $[P_2Se_7]^{4-}$ anion is comparable to those of $[P_2Se_6]^{4-}$ and

(22) (a) Kuhs, W. F.; Schulte-Kellinghaus, M.; Kramer, V.; Nitsche, R. *Z. Naturforsch.* **1977**, *32b*, 1100−1101. (b) Maxwell, R.; Lathrop, D.; Franke, D.; Eckert, H. *Angew. Chem., Int. Ed. Engl.* **1990**, *29*, 882−884. (c) Gaudin, E.; Boucher, F.; Evain, M.; Taulelle, F. *Chem. Mater.* **2000**, *12*, 1715−1720.

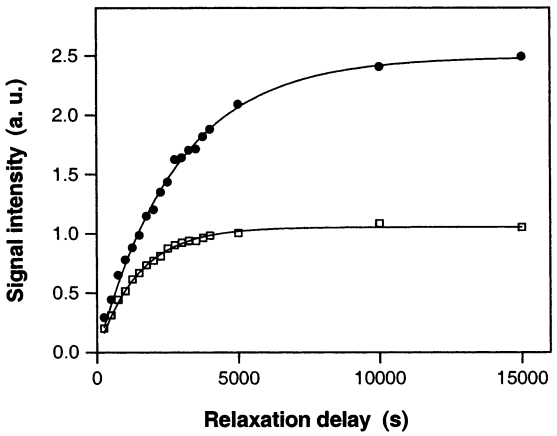

Figure 4. Experimental data and fitting of relaxation times for $Ag_4P_2Se_6$ (solid circles) and Ag_7PSe_6 (open squares). After the magnetization was nulled, there was a variable relaxation delay (τ) followed by a 90° pulse and data acquisition. Signal intensities (in arbitrary units) were calculated as the sum of the integrated isotropic peak and spinning sidebands. Fitting was done using eq 1, and the best-fit curves are superimposed on the experimental data.

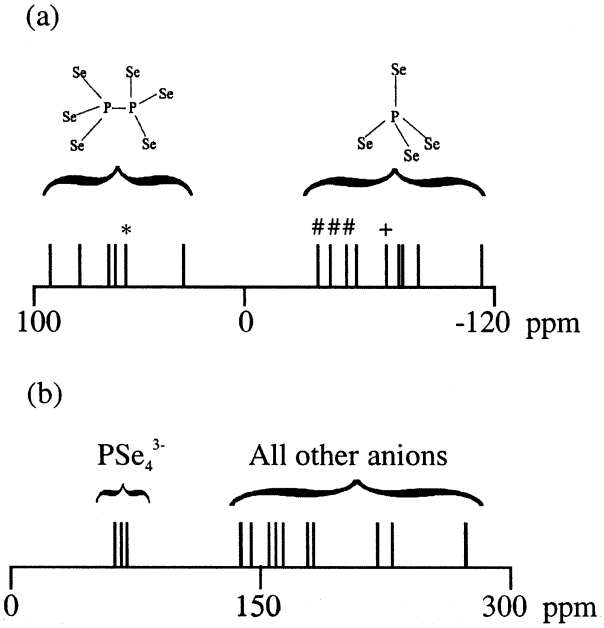

Figure 5. (a) Chemical shifts of selenophosphates containing the anions $[P_2Se_6]^{4-}$, $[PSe_4]^{3-}$, $[P_4Se_{10}]^{4-}$, $[P_2Se_9]^{4-}$, and $[P_2Se_7]^{4-}$. The asterisk indicates the selenophosphate containing the $[P_4Se_{10}]^{4-}$ anion, the number sign indicates the selenophosphates containing the $[P_2Se_9]^{4-}$ anion, and the plus sign indicates the selenophosphate containing the $[P_2Se_7]^{4-}$ anion. The braces indicate that the CS is diagnostic of the presence or absence of a P−P bond. (b) Comparison between the CSAs for compounds with the $[PSe_4]^{3-}$ anion and the CSAs for compounds containing all the other anions. Each CSA was calculated as the difference $\delta_{11} - \delta_{33}$.

$[P_2Se_9]^{4-}$ anions and is significantly larger than those of $[PSe_4]^{3-}$ anions. The CS assignment for $Rb_4Ti_2P_6Se_{25}$ were made using the work of Eckert et al.[23b,24] There are similar T_1 values for the compounds containing the $[P_2Se_7]^{4-}$ anion and/or $[P_2Se_9]^{4-}$ anions.

Correlation of CS, CSA, and T_1 with Ligand Type. The chemical shift discrimination for the selenophosphates is better than that of their thiophosphate counterparts.[23] Figure 5a displays all of the measured CSs on a single ppm scale. As shown in the figure, there is a correlation between the presence of a P−P bond and a downfield CS. The $[P_2Se_6]^{4-}$ and $[P_4Se_{10}]^{4-}$ compounds have positive CSs while the $[PSe_4]^{3-}$, $[P_2Se_7]^{4-}$, and $[P_2Se_9]^{4-}$ compounds have negative CSs. It may also be that the $[P_2Se_9]^{4-}$ CSs are somewhat downfield of the $[PSe_4]^{3-}$ and $[P_2Se_7]^{4-}$ CSs.

For a given anion type, isostructural compounds which only differed in alkali metal ion had ^{31}P CSs within 2 ppm of each other and CSAs within 10 ppm of each other (e.g. $Rb_2CdP_2Se_6/K_2CdP_2Se_6$ and $RbPbPSe_4/KPbPSe_4$). Thus, the CSs and CSAs appear to have only minor dependence on substitution of a metal ion within the same group. By contrast, $K_4Pb(PSe_4)_2$ has the same elements and anion type ($[PSe_4]^{3-}$) as $KPbPSe_4$ but their CSs differ by 39 ppm. All of these observations are probably reasonable because the electronic structure around ^{31}P and thus the corresponding CSs and CSAs should largely depend on local molecular structure.

Figure 5b displays all of the measured CSAs on a single ppm scale. The $[PSe_4]^{3-}$ CSAs are significantly smaller than those of other ligands, presumably because of the unique tetrahedral symmetry of the $[PSe_4]^{3-}$ anion. For compounds containing $[P_2Se_6]^{4-}$ anions, the smallest CSAs were found for $Pb_2P_2Se_6$ and $Ag_4P_2Se_6$. This may be due to the presence of one cation type in these solids compared to two cation types in $Rb_2CdP_2Se_6$ and $K_2CdP_2Se_6$.

The T_1 values for compounds with $[P_2Se_7]^{4-}$ and $[P_2Se_9]^{4-}$ units were clustered between 600 and 800 s, while those for compounds with $[P_2Se_6]^{4-}$ units ranged between 20 and 3000 s and those for compounds with $[PSe_4]^{3-}$ units ranged between 300 and 1500 s. Similar to the CS and CSA, isostructural pairs such as $Rb_2CdP_2Se_6/K_2CdP_2Se_6$ and $RbPbPSe_4/KPbPSe_4$ exhibit T_1 values which are close to one another. However, unlike the CS, T_1 does not appear to correlate with P−P bonding. There may be a variety of interactions which contribute to ^{31}P relaxation, including homo- and heteronuclear dipolar couplings.[25] The experimental correlation between $1/T_1$ and the square of the dipolar coupling is at most qualitative, not quantitative, so there are likely other factors which affect relaxation. As one example, although none of the compounds are paramagnetic per se, there could be small quantities of trapped paramagnetic impurities or defects which contribute to relaxation. To test this hypothesis, we resynthesized the fast-relaxing $Rb_2CdP_2Se_6$ with the idea that paramagnetic reactant concentrations could vary between reactant batches and, thus, produce different T_1 values in the final product. The T_1 value for the resynthesized $Rb_2CdP_2Se_6$ is 70 s, which is close to but not the same as its value in the first synthesis. In future studies, we will attempt to detect paramagnetic impurities using electron spin resonance.

(23) (a) Schmedt auf der Gunne, J.; Eckert, H. *Chem.—Eur. J.* **1998**, *4*, 1762−1767. (b) Regelsky, G. Ph.D. Dissertation, University of Muenster, 2000.
(24) Derstroff, V.; Tremel, W.; Regelsky, G.; Schmedt auf der Gunne, J.; Eckert, H. *Solid State Sci.* **2002**, *4*, 731−745.
(25) Harris, R. K. *Nuclear Magnetic Resonance Spectroscopy*; Wiley: New York, 1987.

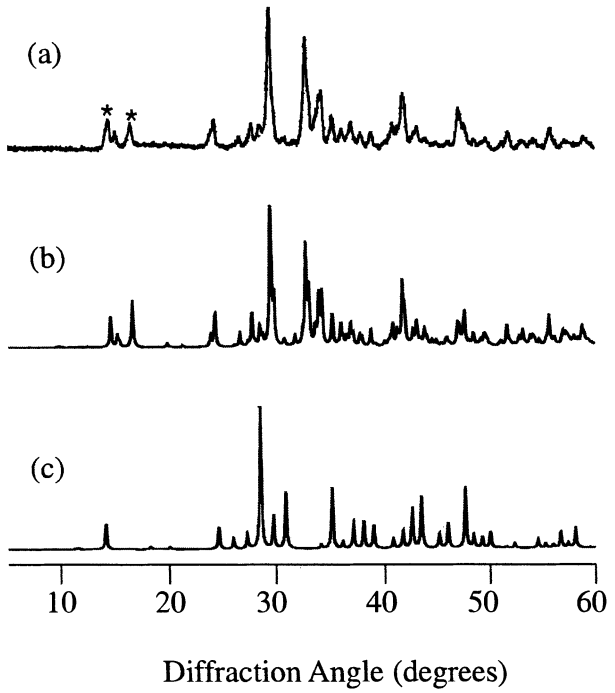

Figure 6. Comparison of the experimental X-ray powder diffraction patterns of the synthesized $Ag_4P_2Se_6$ and the calculated patterns of $Ag_4P_2Se_6$ and Ag_7PSe_6: (a) experimental X-ray powder pattern; (b) calculated X-ray powder pattern for $Ag_4P_2Se_6$; (c) calculated X-ray powder pattern for Ag_7PSe_6. The asterisks in (a) indicate peaks whose relative intensities are not consistent with the calculated $Ag_4P_2Se_6$ pattern.

Impurity Identification with Solid State NMR. Figure 2d displays the spectrum of $Ag_4P_2Se_6$ and Ag_7PSe_6 products formed in a single synthesis. Because the 15000 s delay time was much longer than the T_1 value of either compound, the integrated intensities are quantitative and give a $Ag_4P_2Se_6$:Ag_7PSe_6 product ratio of ~5:1. Observation of sharp lines strongly indicates the presence of crystalline domains of each compound rather than glass formation. In fact, an X-ray analysis of one of the crystals produced in the synthesis gave the $Ag_4P_2Se_6$ structure. Interestingly, the presence of the large Ag_7PSe_6 impurity was also not evident in X-ray powder diffraction analysis of the entire reaction product. Figure 6a displays the experimental powder diffraction pattern while Figure 6b displays the pattern simulated from the known $Ag_4P_2Se_6$ structure. The good agreement between experiment and simulation initially caused confusion in the assignment of the NMR spectrum. After identification of the Ag_7PSe_6 impurity, the powder diffraction data were reexamined and two peaks were found in the experimental pattern whose anomalous relative intensities could be explained by a contribution from Ag_7PSe_6 (cf. Figure 6a,c). However, because of the strong overlap of the Ag_7PSe_6 and $Ag_4P_2Se_6$ powder diffraction patterns, the presence of the Ag_7PSe_6 impurity was generally masked in the experimental pattern. In contrast, the presence of Ag_7PSe_6 is clearly evident in the NMR spectrum because Ag_7PSe_6 contains a $[PSe_4]^{3-}$ anion rather than a $[P_2Se_6]^{4-}$ anion and its CS is more than 100 ppm upfield of $Ag_4P_2Se_6$. Thus, for these selenophosphate syntheses, NMR can be a powerful complementary tool for product identification and analysis.

Interestingly, repeated attempts to synthesize pure $Ag_4P_2Se_6$ always yielded ~20% Ag_7PSe_6 impurity. This was the case even when the reaction was carried out using the $Ag_4P_2Se_6$ stoichiometry. These results suggest that an equilibrium exists between $[P_2Se_6]^{4-}$ and $[PSe_4]^{3-}$ under the 600 °C synthesis melt conditions and that the equilibrium constant is close to 1. Future high-temperature NMR studies will determine the conditions which favor formation of $Ag_4P_2Se_6$ or Ag_7PSe_6 and will follow up on work by Eckert et al., which showed the presence of $[P_2Se_6]^{4-}$ and $[PSe_4]^{3-}$ units in M−P−Se melts (M = Li, Ag).[11]

Our data show other examples of the utility of NMR in analyzing the products of a selenophosphate synthesis. For example, for Figure 2k, the intention of the synthesis was to produce $RbTiPSe_5$ using a procedure and stoichiometry analogous to that employed for $KTiPSe_5$.[20] The NMR spectrum revealed that a pure product was formed, but it was $Rb_4Ti_2P_6Se_{25}$ rather than the intended compound. In the $RbPbPSe_4$ synthesis, impurities are clearly present in the spectrum (cf. Figure 2g) but their chemical identification has not yet been done. Finally, for spectra from some failed syntheses, broad signals were observed which indicate glass rather than crystalline product formation.

In summary, the main result of this study is that the ^{31}P CS is correlated with the presence of P−P bonding in selenophosphate compounds. There are nonoverlapping CS ranges of compounds with P−P bonds (20−100 ppm) and compounds without P−P bonds (−120 to −30 ppm). Thus, in future high-temperature studies of metal−selenophosphate melts, the ^{31}P CS should be useful in ligand identification. It may also be possible to use the CS to distinguish between similar ions in a melt, such as $[P_2Se_7]^{4-}$ and $[P_2Se_9]^{4-}$ anions. CSA measurements demonstrated that the CSAs of compounds containing $[PSe_4]^{3-}$ units were significantly smaller than those of compounds containing any other ion. These other compounds include those with complex ions such as $[P_2Se_7]^{4-}$ and $[P_2Se_9]^{4-}$ which are bridged forms of dimeric $[PSe_4]^{3-}$. These CSA observations are most reasonably explained by the tetrahedral symmetry which is unique to $[PSe_4]^{3-}$ units. The T_1 values of the selenophosphate compounds varied between 20 and 3000 s, but there was no clear correlation with P−P bonding. Finally, ^{31}P NMR was shown to be a useful tool for impurity detection and identification in selenophosphate syntheses.

Acknowledgment. We acknowledge Dr. Jennifer A. Aitken and Ratnasabapathy G. Iyer for useful comments and discussion on the syntheses. We acknowledge Dr. Larry Beck and Kathryn Hughes of the University of Michigan for help on the 7 T NMR measurement and Dr. Robert Tycko at NIH for the Herzfeld−Berger computer program. We acknowledge R. G. Iyer, M. L. Bodner, P. D. Parkanzky, R. Boes, and R. Yang for their assistance with preparation of the cover art. We acknowledge support from NSF Grant DMR-9977650. D.P.W. acknowledges support from a Camille and Henry Dreyfus Foundation New Faculty Award.

IC025946J